

# First Exclusive Measurement of Deep Virtual Compton Scattering off $^4\text{He}$ : Toward the 3D tomography of nuclei

M. Hattawy,<sup>1,2</sup> R. Dupré,<sup>1,2</sup> N.A. Baltzell,<sup>1,3</sup> and K. Hafidi<sup>1,\*</sup>  
(The CLAS Collaboration)

<sup>1</sup>Argonne National Laboratory, Argonne, Illinois 60439

<sup>2</sup>Institut de Physique Nucléaire, CNRS/IN2P3 and Université Paris Sud, Orsay, France

<sup>3</sup>Thomas Jefferson National Accelerator Facility, Newport News, Virginia 23606

(Dated: January 24, 2017)

We report the first exclusive measurements of deeply virtual Compton scattering (DVCS) off a nucleus, where all the products of the reaction including the recoil  $^4\text{He}$  nucleus were detected. The experiment was performed using the Jefferson Lab CEBAF Large Acceptance Spectrometer (CLAS) enhanced with a radial time projection chamber (RTPC) to detect the recoiling  $^4\text{He}$  nuclei. We measure large beam spin asymmetries comparable to the proton's ones and extract in a model independent way, the single chirally-even generalized parton distribution of the  $^4\text{He}$  nucleus. These are pioneering measurements and will lead the way toward the 3D imaging of the partonic structure of nuclei.

PACS numbers: Valid PACS appear here

A wealth of information on the quantum chromodynamics (QCD) structure of hadrons lies in the correlations between the momentum and spatial degrees of freedom of the fundamental constituent partons, quarks and gluons. Such correlations are accessible via the generalized parton distributions (GPDs). The GPDs correspond to the coherence between quantum states of different (or same) helicity, longitudinal momentum, and transverse position. In an impact parameter space, they can be interpreted as a distribution in the transverse plane of partons carrying a certain longitudinal momentum [1–3]. A crucial feature of GPDs is the access to the transverse position of partons which, combined with their longitudinal momentum, leads to the total angular momentum of partons [4]. Deep virtual Compton scattering (DVCS) corresponding to hard exclusive electroproduction of a real photon, which is considered as the cleanest probe to access GPDs and thus study the 3D imaging of nucleons and nuclei.

DVCS measurements have been the focus of a worldwide effort [5–15] involving several accelerator facilities such as Jefferson Lab (JLab), HERA and CERN. The vast majority of the experiments focused on the study of the nucleon's structure. The deuterium was also investigated at HERMES and JLab [16] mainly as a neutron target. However, studying the 3D imaging of the nucleon is a very important goal, understanding how these distributions are modified to provide the binding and structure in a nucleus is as fascinating of a question and an integral part of our quest of using QCD to explore nuclear matter.

A DVCS process on a nuclear target differ from sin-

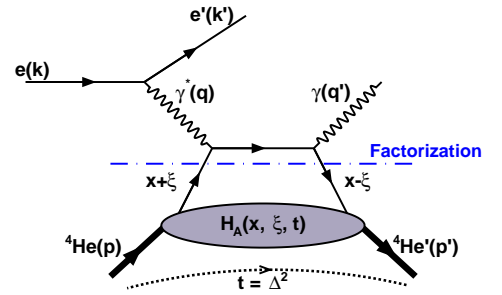


FIG. 1: Representation of the leading-order, twist-2, handbag diagram of the DVCS process off  $^4\text{He}$ .

gle nucleon scattering in providing access to the measure two DVCS channels. In the coherent DVCS channel, the target nucleus ( $A$ ) remains intact and recoils as a whole while emitting a real photon ( $eA \rightarrow e'A'\gamma$ ), allowing to measure the nuclear GPDs of the target. In the incoherent channel, the nucleus breaks up and the DVCS takes place on a bound nucleon ( $N$ ) that emits the final photon ( $eA \rightarrow e'N'\gamma X$ ), enabling the GPDs measurement of the bound nucleons and to study their modifications in the nuclear medium via the GPDs. Figure 1 illustrates the dominant mechanism for the coherent DVCS channel on  $^4\text{He}$ . At sufficiently large squared electron momentum transfer  $Q^2 (= -(k - k')^2)$  and small squared momentum transfer  $t (= (p - p')^2)$ , the QCD factorization theorem predicts that the DVCS handbag diagram can be factorized into two parts, hard and soft parts [17, 18]. The hard part includes photons-quark interaction and it is calculable through perturbative methods, while the soft/non-perturbative part is parametrized in terms of GPDs, which embed the partonic structure of the hadron.

\*corresponding author: kawtar@anl.gov

The GPDs are defined for each quark flavor and gluon as matrix elements of the light cone operators [19], describing the transition between the initial and final states of a hadron. The GPDs depend on two longitudinal momentum fraction variables ( $x, \xi$ ) and on the momentum transfer  $t$  to the target.  $x$  is the average longitudinal momentum fraction of the parton involved in the process and  $\xi$  is the longitudinal fraction of the momentum transfer  $t$ , which is related to the Bjorken variable  $x_B$ :  $\xi \approx \frac{x_B}{2-x_B}$ , where  $x_B = \frac{Q^2}{2M\nu}$  with the proton mass  $M$  and  $\nu = E_e - E_{e'}$ . The GPDs  $x$  variable cannot be measured experimentally in a DVCS reaction. Hence, we measure their convolutions on  $x$ , the so-called Compton Form Factors (CFF) [20]. In a DVCS process, the number of GPDs needed to parametrize the partonic structure of a hadron depends on the different configurations between the spin of the hadron and the helicity direction of the struck quark. Therefore, the partonic structure of spin zero nuclei, such as  $^4\text{He}$  and  $^{12}\text{C}$ , is parametrized by only one GPD ( $H_A(x, \xi, t)$ ) at leading twist, while 4 GPDs arise in the nucleon case. In this work, we have chose the  $^4\text{He}$  nucleus as our target of interest because of its spinless nature and it shows a clear EMC effect [21], in addition of having a high density and it is a well-known few-body system.

The study of nuclear DVCS is still in its infancy due to the challenging detection of the low-energy recoil nuclei in fixed target experiments. Until very recently, the HERMES experiment [26] was the only one to measure DVCS off heavier nuclei such as  $^4\text{He}$ , N, Ne, Kr and Xe, where only the scattered electron and the real photon are detected. In this paper, we report the first exclusive measurements of the coherent DVCS channel off  $^4\text{He}$  where all products of the reaction are detected including the recoiling  $^4\text{He}$  nucleus. Following this exclusive measurement, the  $^4\text{He}$  CFF ( $\mathcal{H}_A$ ) will be extracted experimentally in a fully model independent way for the first time ever. The incoherent DVCS channel measurement from the same data set in in preparation and will reported in another publication.

This work presents the first exclusive measurement of the beam-spin asymmetry of the reaction  $e\ ^4\text{He} \rightarrow e'\ ^4\text{He} \gamma$ . This DVCS sensitive observable is measurable using a polarized lepton beam on an unpolarized target (U). It is convenient to use the beam-spin asymmetry as a DVCS observable because most of the experimental normalization and acceptance issues cancel out in the asymmetry ratio. It is defined in terms of the cross sections as:

$$A_{LU} = \frac{d^5\sigma^+ - d^5\sigma^-}{d^5\sigma^+ + d^5\sigma^-}. \quad (1)$$

where  $d^5\sigma^+ (d^5\sigma^-)$  is the DVCS differential cross section for a positive (negative) beam helicity. Experimentally, the DVCS reaction is indistinguishable from the Bethe-Heitler (BH) process, where the final photon is emitted

either from the incoming or the outgoing leptons. The BH process is not sensitive to GPDs and does not carry information about the partonic structure of the hadronic target, and its amplitude is calculable from the well-known electromagnetic form factors.

The photon-electroproduction cross section can be decomposed into a BH, a DVCS, and an interference terms. At leading twist, the amplitudes of the three terms can be decomposed into a finite sum of Fourier harmonics, the so-called BMK formalism, as shown for the nucleon DVCS in [23] and for the spinless nuclei in [24, 25]. Therefore, the beam-spin asymmetry ( $A_{LU}$ ) with the two opposite helicities of a longitudinally-polarized electron beam (L) on a spin-zero target (U) can be written as:

$$A_{LU}(\phi) = \frac{\alpha_0(\phi) \Im m(\mathcal{H}_A)}{\alpha_1(\phi) + \alpha_2(\phi) \Re e(\mathcal{H}_A) + \alpha_3(\phi) (\Re e(\mathcal{H}_A)^2 + \Im m(\mathcal{H}_A)^2)} \quad (2)$$

where  $\Im m(\mathcal{H}_A)$  and  $\Re e(\mathcal{H}_A)$  are the imaginary and real parts of the  $^4\text{He}$  CFF  $\mathcal{H}_A$  associated to the GPD  $H_A$ . The  $\alpha_i$ 's are  $\phi$ -dependent kinematical factors that depend on the nuclear form factor ( $F_A(t)$ ) and the independent variables  $Q^2$ ,  $x_B$  and  $t$ . These factors are simplified as:

$$\alpha_0(\phi) = \frac{x_A(1+\epsilon^2)^2}{y} S_{++}(1) \sin(\phi) \quad (3)$$

$$\alpha_1(\phi) = c_0^{BH} + c_1^{BH} \cos(\phi) + c_2^{BH} \cos(2\phi) \quad (4)$$

$$\alpha_2(\phi) = \frac{x_A(1+\epsilon^2)^2}{y} (C_{++}(0) + C_{++}(1) \cos(\phi)) \quad (5)$$

$$\alpha_3(\phi) = \frac{x_A^2 t(1+\epsilon^2)^2}{y} \mathcal{P}_1(\phi) \mathcal{P}_2(\phi) \cdot 2 \frac{2-2y+y^2+\frac{\epsilon^2}{2}y^2}{1+\epsilon^2} \quad (6)$$

Where  $S_{++}(1)$ ,  $C_{++}(0)$ , and  $C_{++}(1)$  are the Fourier harmonics in the leptonic tensor. Their explicit expressions can be found in [25]. Therefore, Using the  $\alpha_i$  factors, one can obtain in a totally model-independent way  $\Im m(\mathcal{H}_A)$  and  $\Re e(\mathcal{H}_A)$  from fitting the experimental  $A_{LU}$  as a function of  $\phi$ , the azimuthal angle between the  $(e, e')$  and  $(\gamma^*, ^4\text{He}')$  planes, for given values of  $Q^2$ ,  $x_B$ , and  $t$ .

The experiment, CLAS-EG6, took place in the experimental Hall-B of Jefferson laboratory (JLab) in 2009. JLab delivers, simultaneously, a nearly 100% duty factor polarized electrons into three experimental Halls (A, B, C). The data were collected over three months via projecting a 6.064 GeV longitudinally polarized beam, (83% polarization), on a 6 atm gaseous  $^4\text{He}$  target. The Hall-B Large Acceptance Spectrometer (CLAS) basic design [22] was supplemented, during the CLAS-E1DVCS1 experimental run [11] in 2005, with a specially designed electromagnetic calorimeter, Inner calorimeter (IC). The IC has extended the photon detection acceptance of CLAS, which is originally from  $15^\circ$  to  $45^\circ$ , to polar angle reach as minimum as  $4^\circ$ . During the same experiment, a 5 Tesla solenoid was added around the target to shield the inner detectors from the low-energy Møller electrons.

At 6 GeV incident electron beam energy, the recoil  $^4\text{He}$  nuclei, from the coherent DVCS channel, have an aver-

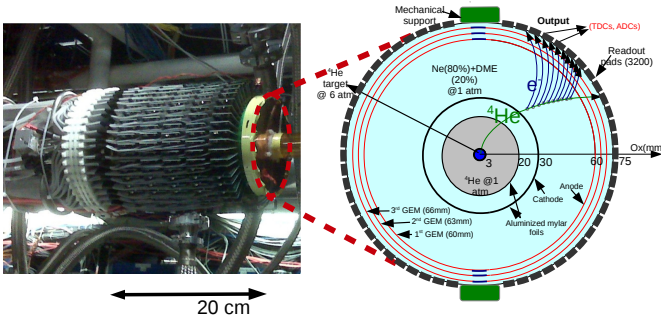


FIG. 2: Left: A picture of the CLAS-EG6 RTPC before insertion into the solenoid. Right: A cross section of the CLAS-EG6 RTPC perpendicular to the beam direction. An illustration of a  $^4\text{He}$  track originating from the pressurized straw target is shown along with the electrons produced in the drift region.

age momentum (per charge) around 125 MeV/c, while the CLAS spectrometer detects charged particles with a threshold of 250 MeV/c. In order to ensure the exclusivity of the our coherent DVCS channel, we built a small and light radial time projection chamber (RTPC) to detect recoiling nuclei down to energies of few MeVs. Figure 2 presents our cylindrical RTPC, which is 20 cm long and 15 cm diameter, surrounding the  $^4\text{He}$  gaseous target and being inside the available space inside the solenoid, with a 3 cm radial drift length. The detector was specifically calibrated for  $^4\text{He}$  nuclei using elastic scattering produced with a 1.2 GeV electron beam.

Identifying the coherent DVCS candidates is the first step of the data analysis. These events have one electron, one  $^4\text{He}$ , and at least one photon in the final state. Electrons were identified by passing the fiducial cuts and having signals in all the sub-detectors of CLAS spectrometer (drift chambers, Cherenkov counters, the standard CLAS electromagnetic calorimeter, and scintillators).  $^4\text{He}$  tracks were identified by passing all the geometrical, timing and quality cuts in the RTPC detector. In principle, with constant beam luminosity, target density and pressure, the event rate has to be constant over the experimental time. Due to the changes in the experimental conditions, such as changing a trigger in a detector, a slight shift in the beam position or a system failure somewhere, this rate changes. We minimize the effects of these changes on the reconstructed events by selecting the good runs. To this aim, we monitor the ratio between the number of the good tracks reconstructed in the RTPC to number of the detected good electrons in the CLAS detector as a function of run number [27].

Even though the DVCS reaction has only one real photon in the final state, events with more than one good

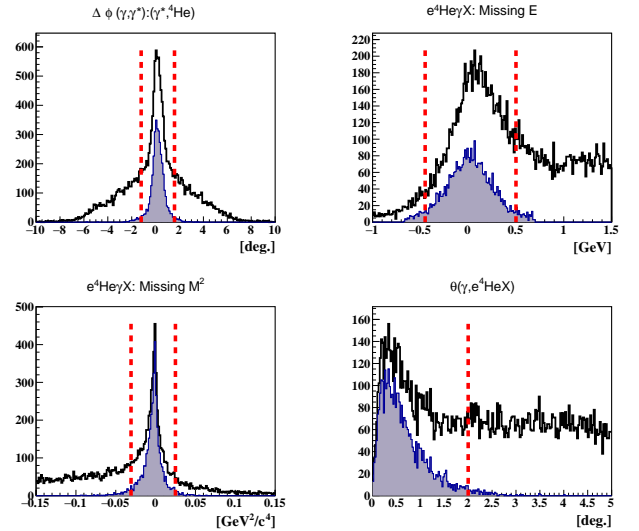


FIG. 3: Four of the seven coherent DVCS exclusivity cuts. The black distributions represent the coherent DVCS events candidate. The shaded distributions represent the events which passed all the exclusivity cuts except the quantity plotted. The vertical red lines represent the applied exclusivity cuts. The distributions from left to right and from top to bottom are:  $\Delta\phi$ , missing energy and missing mass squared in  $e^4\text{He}\gamma X$ , and the cone angle ( $\theta$ ) between the measured and the calculated photons.

photon are not discarded at this stage. This is motivated by the fact that some photons correspond to random coincidences and discarding these events results in losing good events. Then, events with one or more  $\pi^0$  are removed from the coherent DVCS sample. After that, the most energetic IC photon was considered as the DVCS photon candidate. Next, a  $Q^2 > 1 [\text{GeV}^2/c^2]$  cut is applied on the DVCS candidates in order to ensure that the interaction occurs at the partonic level and the applicability of the factorization in the DVCS handbag diagram. Once the three final state particles were identified with their 3-momentum vectors, the exclusivity of the coherent DVCS events were ensured by applying a set of exclusive cuts, which are: the co-planarity angle ( $\Delta\phi$ ), missing energy, missing mass squared and missing transverse momentum in the  $e^4\text{He}\gamma X$  final state configuration, the missing mass squared in the  $e^4\text{He}'X$  and  $e'\gamma X$  configurations, and finally the cone angle ( $\theta$ ) between the measured real photon and the missing particle in the  $e^4\text{He}'X$  configuration. Figure 3 presents four of the applied exclusivity cuts, where  $3\sigma$  cuts are applied on all the exclusive quantities except the missing energy, for which a  $[-0.45, 0.5] \text{ GeV}$  cut was adopted to reduce the background contribution. Finally,

After all the requirements on the individual final state particles of the coherent DVCS events and the exclusivity cuts, we ended up with about 3500 events. Figure 4 presents the  $(Q^2, x_B)$  and  $(Q^2, -t)$  kinematic coverage of

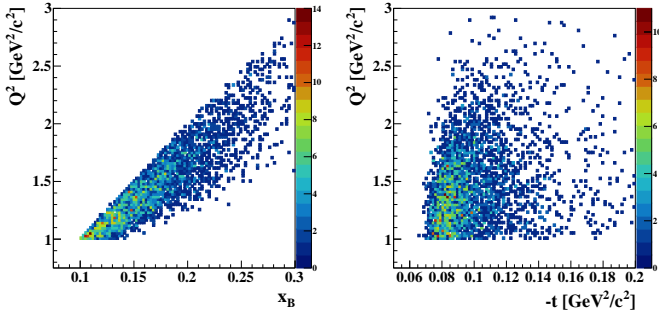


FIG. 4: The  $Q^2$  as a function of  $x_B$  (left) and the  $Q^2$  as a function of  $-t$  (right) for the identified coherent DVCS events after the exclusivity cuts.

the collected DVCS events.

Even with all the previously presented exclusive cuts, the selected events are not all true DVCS events. We identified several background contributions to the coherent DVCS process, in particular accidental events and exclusive Deeply Virtual  $\pi^0$  Production (DV $\pi^0$ P). The accidental events where the different particles come from different events are suppressed by the limited phase space allowed by the exclusivity cuts. We estimate the accidental events to represent 4.1% of our sample. This relatively large number is due to the small cross section of the DVCS. We evaluated this contribution by selecting events passing all our cuts but with particles originating from different vertices. Regarding the DV $\pi^0$ P, which can easily be mistaken with DVCS when one of the two photons of the  $\pi^0$  decay is produced at low energy in the laboratory frame. To estimate the importance of this background, we developed an event generator that we calibrated to match our measured experimental yield of exclusive  $\pi^0$ . We used this generator together with a GEANT3 simulation of our detection system to estimate the ratio of acceptance between DV $\pi^0$ P where the two photons are detected and those where only one photon is detected and would pass our DVCS selection cuts. This ratio obtained from simulation is then multiplied by the measured yield of DV $\pi^0$ P events, indicating a contamination of 2 to 4%. The study of systematic errors showed that the main contributions come from the choice of the DVCS exclusivity cuts (8%) and the large binning size (5.1%). However added quadratically, these errors sum up to 10%, which remain for all bins well below the statistical errors.

$A_{LU}$  can be simplified in terms of the collected number of events in each beam-helicity state ( $N^+$ ,  $N^-$ ) as:

$$A_{LU} = \frac{1}{P_B} \frac{N^+ - N^-}{N^+ + N^-}. \quad (7)$$

where  $P_B$  is the beam polarization, and  $N^+$  and  $N^-$  are the number of DVCS events detected with positive

and negative electron helicity with respect to the beam direction. The statistical uncertainty of  $A_{LU}$  is

$$\sigma_{A_{LU}} = \frac{1}{P_B} \sqrt{\frac{1 - (P_B A_{LU})^2}{N}} \quad (8)$$

where  $N(N^+ + N^-)$  is the total number of measured events.

Due to our limited statistics only, a two-dimensional binning is carried out in this work. The strongest dependence of  $A_{LU}$  is on the azimuthal angle ( $\phi$ ). Thus, the coherent measured ranges of  $Q^2$ ,  $x_B$  and  $t$  are binned statistically into three bins. Then, the identified DVCS events in each bin are binned into nine bins in  $\phi$ . Therefore, we are left with  $Q^2$ - $\phi$  bins integrated over the full ranges of  $x_B$  and  $t$ ,  $x_B$ - $\phi$  bins integrated over  $Q^2$  and  $t$ , and  $t$ - $\phi$  bins integrated over  $Q^2$  and  $x_B$ .

Figure 5 presents the coherent  $A_{LU}$  for the three sets of two-dimensional bins. The asymmetries are fitted with the form of equation 2, where the real and the imaginary part of the CFF  $\mathcal{H}_A$  are the free parameters in the fit. Figure 6 shows the  $Q^2$ ,  $x_B$ , and  $-t$  dependencies of the fitted  $A_{LU}$  signals at  $\phi = 90^\circ$ . The  $x_B$  and  $-t$  dependencies are compared to theoretical calculations performed by S. Liuti and K. Taneja [28]. Their model relies on the impulse approximation and uses advanced spectral function of the nuclei to calculate the nuclear GPDs and then the observables. The calculations were carried out at slightly different kinematics than ours but provide already some guidance. The experimental results appear to have larger asymmetries compared to the calculations. These differences may arise from nuclear effects which are not taken into account in the model, such as long-range interactions. Our measurements also agree with those of HERMES, considering their large uncertainties.

As has been advertised previously, the  $^4\text{He}$  CFF  $\mathcal{H}_A$  can be extracted from fitting the experimentally measured coherent  $A_{LU}$  in a totally model independent way, which is not the case of nucleon targets. For the later, four CFFs exist and extracting them is always made by making limitations according some theoretical models and by neglecting some CFFs [15]. Figure 7 presents our extracted imaginary and real parts of the CFF  $\mathcal{H}_A$  as function of the kinematical variable ( $Q^2$ ,  $x_B$ ,  $-t$ ), and compared to some theoretical calculations.

We display in figure 7 calculations for  $\mathcal{H}_A$  from three GPD models: On-shell, Convolution, and off-shell models. In the On-shell model [30], a nucleus is assumed to be composed of non-relativistic non-interacting nucleons, and these nucleons interact independently with the probe. For the nucleons, the GPDs are modeled according to the dual parametrization [31]. In the Convolution model, the same assumption has been made for the nucleus, while the nucleon GPDs were extracted from the VGG model, which is based on the double distributions

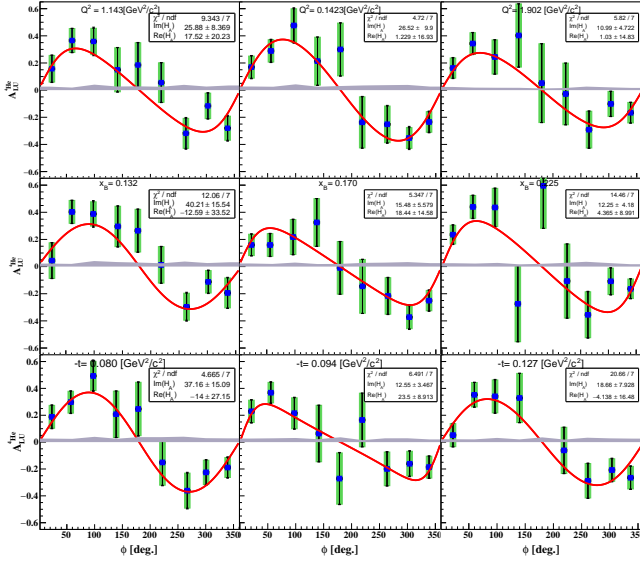


FIG. 5: The coherent  $A_{LU}$  as a function of  $\phi$  in  $Q^2$  (top panel),  $x_B$  (middle panel), and  $-t$  (bottom panel) bins. The error bars represent the statistical and the systematic uncertainties added quadratically, shown on top in green are error bars representing only the statistical uncertainties. The bluish-gray bands represent the systematic uncertainties, including the normalisation systematic uncertainties. The red curves represent fits in the form of equation 2.

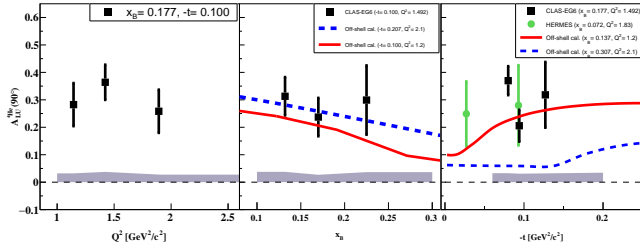


FIG. 6: The  $Q^2$  (left),  $x_B$  (middle), and  $-t$ -dependencies (right) of the coherent  $A_{LU}$  at  $\phi = 90^\circ$  (black squares). On the middle plot: the full-red and the dashed-blue curves are theoretical calculations from [28]. On the right: the green circles are the HERMES  $-A_{LU}$  (positron beam was used) inclusive measurements [29], the colored curves represent theoretical calculations from [28].

ansatz [33]. The Off-shell model [34] relies on the impulse approximation also, but uses advanced spectral function of the nuclei that accounts for all configurations of the final nuclear system and the binding effects between the nucleons.

In figure 7, within the given uncertainties, the extracted CFF shows a slight dependence on  $Q^2$ ,  $x_B$ , and  $-t$ , which are in agreement with the theoretical calculations. One can see a difference between the precision of the extracted imaginary and real parts, which is expected

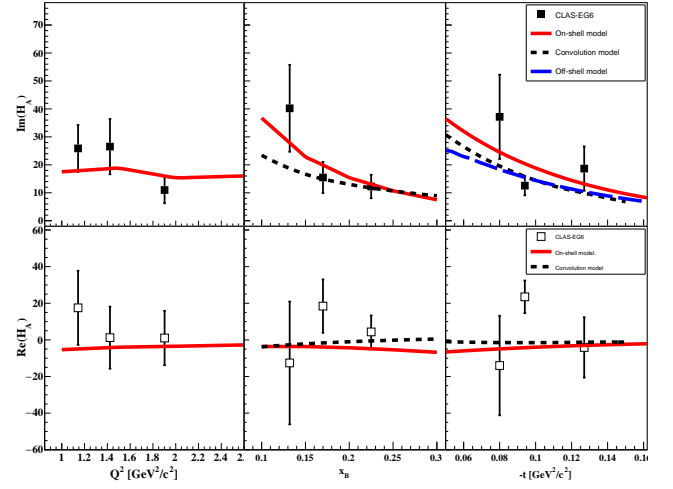


FIG. 7: The model-independent extraction of the imaginary (top panel) and real (bottom panel) parts of the  $^4\text{He}$  CFF  $\mathcal{H}_A$ , as functions of  $Q^2$  (right panel),  $x_B$  (middle panel), and  $t$  (left panel). The full red curves are calculations based on an on-shell model from [30]. The black-dashed curves are calculations from a convolution model based on the VGG model for the nucleons' GPDs [32]. The blue long-dashed curve on the top-right plot is from an off-shell model based on [34].

because  $\alpha_2$  is suppressed compared to  $\alpha_0$  contribution. However, we note that the error bars are finite and that the fit converge without placing any bound on the CFF, which is necessary on proton targets.

In summary, we presented the first exclusive measurement of the coherent DVCS off  $^4\text{He}$  using CLAS spectrometer, supplemented with an inner calorimeter, a 5 Tesla solenoid, and a specially designed radial TPC. This dataset represents a unique source for the nuclear DVCS global dataset, which will be used to constrain GPD models. The measured beam-spin asymmetries show a very strong signal and allowed to perform the first fully model-independent extraction of the  $^4\text{He}$  CFF  $\mathcal{H}_A$ . The extracted CFFs, while limited by statistics, are in a good agreement with the available GPD models. This opens many new perspectives to study the nuclear structure within the GPDs framework and pave the way for future more precise measurements at JLab 12 GeV program and possibly at the Electron-Ion Collider (EIC) to achieve better understanding of the nuclear effects.

We acknowledge the staff of the Accelerator and Physics Divisions at Jefferson Lab for making this experiment possible. This work is supported by the U.S. Department of Energy, Office of Science, Office of Nuclear Physics contract DE-AC05-06OR23177.



- 
- [1] M. Burkardt, Phys. Rev. D **62**, 071503 (2000) Erratum: [Phys. Rev. D **66**, 119903 (2002)]
- [2] M. Diehl, Eur. Phys. J. C **25**, 223 (2002) Erratum: [Eur. Phys. J. C **31**, 277 (2003)]
- [3] A. V. Belitsky and D. Mueller, Nucl. Phys. A **711**, 118 (2002)
- [4] M. Burkardt, Phys. Rev. D **72**, 094020 (2005)
- [5] S. Stepanyan *et al.* [CLAS Collaboration], Phys. Rev. Lett. **87**, 182002 (2001).
- [6] A. Airapetian *et al.* [HERMES Collaboration], Phys. Rev. Lett. **87**, 182001 (2001); JHEP **1207**, 032 (2012); JHEP **1006**, 019 (2010); JHEP **0806**, 066 (2008); Phys. Lett. B **704**, 15 (2011); Phys. Rev. D **75**, 011103 (2007); JHEP **0911**, 083 (2009); Phys. Rev. C **81**, 035202 (2010); JHEP **1210**, 042 (2012).
- [7] S. Chekanov *et al.* [ZEUS Collaboration], Phys. Lett. B **573**, 46 (2003).
- [8] A. Aktas *et al.* [H1 Collaboration], Eur. Phys. J. C **44**, 1 (2005).
- [9] S. Chen *et al.* [CLAS Collaboration], Phys. Rev. Lett. **97**, 072002 (2006).
- [10] C. Muñoz Camacho *et al.* [Jefferson Lab Hall A Collaboration], Phys. Rev. Lett. **97**, 262002 (2006).
- [11] F.X. Girod *et al.* [CLAS Collaboration], Phys. Rev. Lett. **100**, 162002 (2008).
- [12] G. Gavalian *et al.* [CLAS Collaboration], Phys. Rev. C **80**, 035206 (2009).
- [13] E. Seder *et al.* [CLAS Collaboration], Phys. Rev. Lett. **114**, 032001 (2015).
- [14] S. Pisano *et al.* [CLAS Collaboration], Phys. Rev. D **91**, 052014 (2015).
- [15] H. S. Jo *et al.* [CLAS Collaboration], Phys. Rev. Lett. **115**, no. 21, 212003 (2015)
- [16] M. Mazouz *et al.* [Jefferson Lab Hall A Collaboration], Phys. Rev. Lett. **99**, 242501 (2007)
- [17] A. Freund and J.C. Collins, Phys. Rev. D **59**, 074009 (1998)
- [18] X.-D. Ji and J. Osborne, Phys. Rev. D **58**, 094018 (1998)
- [19] A. V. Belitsky and A. V. Radyushkin, Phys. Rept. vol. 418 (2005)
- [20] M. Guidal, H. Moutarde and M. Vanderhaeghen, Rept. Prog. Phys. **76**, 066202 (2013)
- [21] J. Seely *et al.* Phys. Rev. Lett. **103**, 202301 (2009)
- [22] B.A. Mecking *et al.*, Nucl. Inst. and Meth. A 503, 513 (2003)
- [23] A. V. Belitsky, D. Mueller and A. Kirchner, Nucl. Phys. B **629**, 323 (2002)
- [24] A. Kirchner and D. Mueller, Eur. Phys. J. C **32**, 347 (2003)
- [25] A. V. Belitsky and D. Mueller, Phys. Rev. D **79**, 014017 (2009)
- [26] F. Ellinghaus *et al.* [HERMES Collaboration], AIP Conf. Proc. **675**, 303 (2003)
- [27] M. Hattawy *et al.* (CLAS-EG6 Working Group), CLAS internal analysis note, 2016.
- [28] S. Liuti and K. Taneja, Phys. Rev. C **72**, 032201 (2005)
- [29] A. Airapetian *et al.* (HERMES Collaboration), Phys. Rev. C **81**, 035202 (2010)
- [30] Private communications with V. Guzey based on: V. Guzey, Phys. Rev. C **78**, 025211 (2008).
- [31] V. Guzey and T. Teckentrup, Phys. Rev. D **74**, 054027 (2006)
- [32] Private communications with M. Guidal based on: M. Guidal, M. V. Polyakov, A. V. Radyushkin and M. Vanderhaeghen, Phys. Rev. D **72**, 054013 (2005).
- [33] I. V. Musatov and A. V. Radyushkin, Phys. Rev. D **61**, 074027 (2000).
- [34] Private communications with S. Liuti based on: J. O. Gonzalez-Hernandez, S. Liuti, G. R. Goldstein and K. Kathuria, Phys. Rev. C **88**, no. 6, 065206, (2013).